

Collisional excitation of propyne (CH₃CCH) by He atoms

M. Ben Khalifa* B. Darna and J. Loreau

KU Leuven, Department of Chemistry, Celestijnenlaan 200F, B-3001 Leuven, Belgium.
e-mail: malek.benkhalfifa@kuleuven.be, jerome.loreau@kuleuven.be

February 28, 2024

ABSTRACT

Context. A detailed interpretation of the detected emission lines of environments in which propyne (or methyl acetylene, CH₃CCH) is observed requires a knowledge of its collisional rate coefficients with the most abundant species in the interstellar medium, He or H₂.

Aims. We present the first three-dimensional potential energy surface (3D-PES) for the CH₃CCH-He molecular complex, study the dynamics of the collision, and report the first set of rate coefficients for temperatures up to 100 K for the collisional excitation of the lowest 60 *ortho* rotational levels and 60 *para* rotational levels of CH₃CCH by He atoms.

Methods. We computed the 3D-PES with the explicitly correlated coupled-cluster with single-, double-, and perturbative triple-excitation method, in conjunction with the augmented correlation-consistent triple zeta basis set (CCSD(T)-F12a/aug-cc-pVTZ). The 3D-PES was fitted to an analytical function. Scattering computations of pure rotational (de-)excitation of CH₃CCH by collision with He atoms were performed and the state-to-state cross sections were computed using the close coupling method for total energies up to 100 cm⁻¹ and with the coupled states approximation at higher energy for both *ortho* and *para* symmetries of CH₃CCH.

Results. The PES obtained is characterized by a large anisotropy and a potential well depth of 51.04 cm⁻¹. By thermally averaging the collisional cross sections, we determined quenching rate coefficients for kinetic temperatures up to 100 K. A strong even Δj propensity rule at almost all collision energies exists for CH₃CCH-He complex. To evaluate the impact of rate coefficients in the analysis of observations, we carried out non-LTE radiative transfer computations of the excitation temperatures and we demonstrate that LTE conditions are typically not fulfilled for the propyne molecule.

Key words. scattering – ISM: molecules – astrochemistry

1. Introduction

Over the past decades, methyl acetylene (or propyne, CH₃CCH) has received significant attention from the astrophysical and astrochemistry communities due to its important role in astrochemical processes (Mebel et al. 2017; Herbst 2017) such as its role as a precursor in the formation of several polycyclic aromatic hydrocarbons (PAHs) (Parker & Kaiser 2017).

The earliest tentative detection of propyne in the interstellar medium (ISM) was reported toward the Sgr B2 molecular cloud by Buhl & Snyder (1973). Later, propyne was observed by Lovas et al. (1976) towards Orion A and Sagittarius B2 through the 5₀ → 4₀ rotational line at 85 GHz. In the following years, CH₃CCH was identified in various astronomical environments: low mass star-forming regions (van Dishoeck et al. 1995), photodissociation regions through the Horsehead nebula with fractional abundances of 10⁻⁹ with respect to molecular hydrogen (Gratier et al. 2013; Guzmán et al. 2014; Hickson et al. 2016), massive young stellar objects (Fayolle et al. 2015), circumstellar envelopes of evolved stars (Agúndez et al. 2008) and even toward extragalactic sources such as M82, NGC 253, and NGC 1068 (Mauersberger et al. 1991; Qiu et al. 2020). It has also been detected in cold and dense cores (Vastel et al. 2014; Gratier et al. 2016) and even toward a planetary nebula, as recently reported by Schmidt & Ziurys (2019). As a matter of fact, the widespread detection of propyne even extends to planetary atmospheres: in our solar system, CH₃CCH has also been detected on Jupiter, Saturn, Uranus as well as in the atmosphere of Titan (Fouchet

et al. 2000; De Graauw et al. 1997; Burgdorf et al. 2006; Teanby et al. 2009).

The formation pathways of propyne in the gas phase have been widely studied and it has been demonstrated that there are no efficient synthetic pathways in gas-phase available to reproduce the abundances of CH₃CCH in the cold molecular clouds (Hickson et al. 2016). It was proposed that the principal source of propyne in the gas phase is via ion-molecule reactions with C₂H₂⁺ as a precursor (Schiff & Bohme 1979), neutral-neutral reactions such as CCH + CH₄ → CH₃CCH + H (Turner et al. 1999) as well as dissociative recombination reactions involving larger hydrocarbons (Calcutt et al. 2019).

Those pathways were not capable to reproduce the observed abundance of CH₃CCH in the astrophysical media. For this reason, surface reactions occurring on interstellar grains were additionally studied (Hickson et al. 2016; Guzmán et al. 2018). Propyne molecules are believed to adhere to the cold dust grains and then undergo hydrogenation at cold molecular cloud temperature of about 10 K. CH₃CCH was demonstrated to form through the hydrogenation of C₃ radical which could be further hydrogenated to propene. Nevertheless, the model including grain surface and gas phase reactions was not able to reproduce the observed methyl acetylene abundance by more than one order of magnitude. This failure to reproduce the abundance of propyne demonstrate that more crucial formation pathways are still unknown at low temperatures (Hickson et al. 2016; Guzmán et al. 2014; Öberg et al. 2013).

CH₃CCH is a symmetric top molecule and among the most efficient thermometers available. For a given j , the rotational levels

* ,

associated to propyne are split into several levels with different k quantum numbers. Consequently, there are multiple rotational transitions with different k quantum numbers that cover a wide energy range above the ground state, but that are closely spaced in frequency and can therefore all be observed in the same bandwidth: that is, many transitions can be observed simultaneously using the same antenna settings and sensitivities thereby reducing the calibration uncertainties. The dipole moment of propyne is parallel to the C_3 axis, hence, radiative transitions with $\Delta k \neq 0$ are forbidden: different k -components are connected only via collisional process, which makes their relative population sensitive to the kinetic temperature.

The interstellar medium where propyne generally resides is characterized by a very low density, and therefore the populations of its rotational states are usually not in local thermodynamic equilibrium (LTE). Therefore, the analysis of intensities of spectroscopic lines of CH_3CCH requires the application of a radiative transfer model. Such a model requires spectroscopic data for radiative transfer rates, which are usually available, as well as collisional rate coefficients for rotational transitions induced by collisions with the dominant interstellar species, usually He or H_2 , which are often not available. Consequently, these collisional rates must be calculated in quantum scattering computations using a precise potential energy surface (PES) for the interaction of the molecule with He or H_2 .

To the best of our knowledge, no collisional state-to-state rate coefficients are available in the literature and the present set of collisional rate coefficients is the first one obtained by fully quantum methods.

In the present paper, we study the collisional excitation of the rigid symmetric top molecule CH_3CCH with He atoms for temperature up to 100 K. The overall structure of this paper is as follows: section 2 describes the *ab-initio* computation of the 3-dimensional CH_3CCH -He intermolecular potential, the analytical representation of the interaction potential is defined and the potential is illustrated. In Sect. 3 we describe the study of the dynamics, where we illustrate inelastic cross sections in CH_3CCH -He collisions. We discuss rate coefficients for CH_3CCH -He collisions in Sect. 4. We analyze the impact of our rate coefficients by performing a radiative transfer calculation for typical interstellar conditions in Sect. 5. Conclusions and future outlooks are drawn in Sect. 6.

2. Potential energy surface

In this section, we aim to compute the first accurate potential energy surface between a symmetric top molecule, CH_3CCH (X^1A_1), with a structureless helium atom (1S) in their respective electronic ground states.

The 3D-PES was computed as a function of three Jacobi coordinates (R, θ, ϕ) . The origin of the coordinate system is the centre of mass of CH_3CCH molecule and the Z axis lies along its C_3 symmetry axis. R denotes the intermolecular separation between the center of mass of CH_3CCH and He atom and θ and ϕ define the orientation of the He atom. The coordinates defining the geometry of the CH_3CCH -He system are presented in Fig. 1. For $\phi=0^\circ$, the He atom is in the plane formed by the axis of molecule and one of the C-H bonds, while for $\phi=60^\circ$, the He atom is situated at equal distance between two hydrogen atoms.

The propyne molecule was assumed to be rigid in the computation of the interaction potential of CH_3CCH -He where the internal coordinates of CH_3CCH were frozen to the average geometry of the $\nu=0$ vibrational state as follows: $r(H-C)=1.061$ Å, $r(C\equiv C)=1.215$ Å, $r(C-C)=1.458$ Å, $r(C-H)=1.089$ Å and

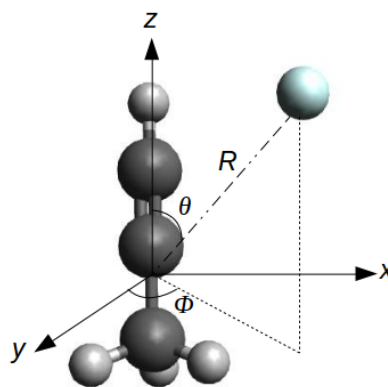


Fig. 1: Jacobi coordinates defining the geometry of the CH_3CCH -He van der Waals complex. The origin of the reference frame is at the CH_3CCH center-of-mass. The angles are defined so that for $\theta=0^\circ$, He approaches along the C-H end of the molecule and for $\phi=60^\circ$, the He atom lies in the plane defined by CHCH atoms on the side of the H atom.

$\angle(HCC)=110.7^\circ$ (El Idrissi et al. 2001).

Explicitly correlated coupled cluster computations with inclusion of single, double, and perturbatively triple excitations [CCSD(T)-F12a] (Knizia et al. 2009) in conjunction with the augmented correlation consistent polarized valence triple zeta (aug-cc-pVTZ) basis sets of Dunning (Dunning Jr 1989) were used to calculate *ab-initio* points on the CH_3CCH -He interaction potential and the MOLPRO code (Werner et al. 2015) was used to perform these computations in the C_1 symmetry group. The performance of such an approach was already tested for CH_3CN -He, CH_3NC -He (Ben Khalifa et al. 2022) as well as SiH_3CN -He (Naouai et al. 2021), and it was proven that CCSD(T)-F12 method supplemented by the aVTZ basis set give an excellent accuracy for interactions involving rare gases. A counterpoise correction of Boys & Bernardi (1970) was considered to correct for the basis set superposition error (BSSE) according to the following expression:

$$V(R, \theta, \phi) = V_{Mol-He}(R, \theta, \phi) - V_{Mol}(R, \theta, \phi) - V_{He}(R, \theta, \phi) \quad (1)$$

where V_{Mol-He} is the global electronic energy of CH_3CCH -He system, and the last two terms are the energies of the two fragments, all performed using the full basis set of the total system. The ranges of variation used to compute the PES was constructed as follows. For the angle θ , the grid is made up of 19 values from 0° to 180° , while for the angle ϕ , we used 7 values from 0° to 60° uniformly distributed by steps of 10° . All other geometries are obtained by symmetry. Finally, for the intermolecular distance R , we used a grid of 60 points ($4 \leq R \leq 50 a_0$). We used a spacing of $0.2 a_0$ in the short-range, while in the long-range, the spacing is increased progressively. These parameters lead to a set of 7980 energy points.

We take into consideration the inconsistency in size of the CCSD(T)-F12a method, thus, the PES computed with this approach was shifted by subtracting the asymptotic value of the PES at $R=50 a_0$, which is equal to -5.3 cm^{-1} .

2.1. Analytical fit

It is useful for the computation of the matrix elements of the interaction between scattering basis functions in time-independent

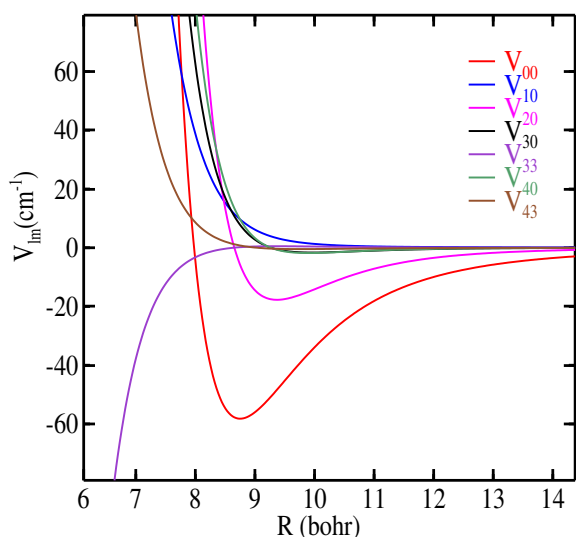


Fig. 2: Dependence on R of the first $V_{lm}(R)$ components for CH₃CCH-He with $0 \leq l \leq 4$.

quantum method to use the functional form presented below:

$$V(R, \theta, \phi) = \sum_{l=0}^{l_{\max}} \sum_{m=0}^l V_{lm}(R) \frac{Y_l^m(\theta, \phi) + (-1)^m Y_l^{-m}(\theta, \phi)}{1 + \delta_{m,0}} \quad (2)$$

where $V_{lm}(R)$ and $Y_l^m(\theta, \phi)$ are the radial coefficients to be computed and the normalized spherical harmonics respectively, and $\delta_{m,0}$ is the Kronecker delta symbol.

Due to the C_{3v} symmetry of the propyne molecule, the values of m are restricted to terms for which m is multiple of 3 ($m = 3n$, n integer) in the expansion.

From a PES grid containing (19,7) values of (θ, ϕ) , we could include radial coefficients up to $l_{\max}=18$ and $m=18$. The total number of expansion coefficients is equal to 70 with a final accuracy better than 1 cm⁻¹ for $R \geq 5$ bohr. Finally, a least-square interpolation was used over the entire range of intermolecular distances to supply continuous expansion coefficients suitable for scattering computations. For $R \geq 30$ bohr, we extrapolated the long-range potential using an inverse exponent expansion implemented in the MOLSCAT (Hutson & Green 1995) computer code.

We present in Fig. 2 the dependence on R of the radial coefficients up to $l=4$. Here, V_{00} represents the isotropic potential, responsible for elastic collisions, while terms with $l \geq 1$ describe the anisotropic part of the PES responsible for inelastic collisions. As one can see, the largest (in magnitude) of the anisotropic terms ($l > 0$) is associated to $l = 2$, a term that is responsible for transitions with $\Delta j=2$. This should have an effect on the propensity rules in the rotational excitation, as discussed in more detail below.

2.2. Analysis of the PES

The global minimum of the PES, which describe the main interaction of CH₃CCH-He, is located at the equilibrium intermolecular separation $R_e=6.3$ bohr with a well depth of $D_e= 51.04$ cm⁻¹. The configuration of the global minimum is defined by

the angles $\phi = 60^\circ$ and $\theta = 104^\circ$, while a local minimum of 37.6 cm⁻¹ is located at $R = 8.6$ bohr and $\theta = 180^\circ$. The global and local minima are separated by a barrier of -27.07 cm⁻¹ that is located at $\theta = 137^\circ$ and $R = 8.35$ bohr.

The internal rotation along the ϕ coordinate is almost free: the energy of the minimum increases between $\phi = 0^\circ$ and $\phi = 30^\circ$ (from -46.8 cm⁻¹ at $\theta = 94^\circ$ to -46.6 cm⁻¹ at $\theta = 98^\circ$) and then decreases between $\phi = 30^\circ$ and $\phi = 60^\circ$ (from -46.6 cm⁻¹ at $\theta = 98^\circ$ to -51.04 cm⁻¹ at $\theta = 104^\circ$). This behavior was already observed for other systems with C_{3v} symmetry such as CH₃CN-He and CH₃NC-He (Ben Khalifa et al. 2022), and is due to the elongated shape of the propyne molecule.

We note that the PES for CH₃CCH-He share the same qualitative behavior previously observed for molecules with a three-fold symmetry axis interacting with rare gas atoms (Gubbels et al. 2012; Loreau et al. 2014; Loreau & Van der Avoird 2015; Ben Khalifa et al. 2022; Naouai et al. 2021) where the global minimum occurs at $\phi=60^\circ$, that is, with the helium atom located between two hydrogen atoms. Because of the C_{3v} symmetry of the CH₃CCH molecule, there are two more symmetry equivalent orientations for the global minimum, at $\phi=180^\circ$ and $\phi=300^\circ$. We illustrate in Fig. 3 (left panel), the two-dimensional cut of the interaction potential as a function of two Jacobi coordinates (R and θ) while the ϕ angle is held fixed at its equilibrium value corresponding to the CH₃CCH-He minimum. The variation in this cut shows a strong anisotropy of the interaction potential of CH₃CCH-He along the θ coordinate. For a better appreciation of the topography of the PES, we present also 2D-cut of the 3D-PES as a function of θ and ϕ for $R = 6.6$ bohr (Fig. 3 right panel). This type of plot offers a unique overview as it includes all minima and the barriers between them.

3. Scattering calculations

CH₃CCH is a prolate symmetric top molecule that belongs to the C_{3v} point group with a dipole moment of 0.7829 Debye (Włodarczyk et al. 1988). The relevant rotational Hamiltonian associated with CH₃CCH is expressed as follow:

$$H_{rot} = \frac{\hbar^2}{2I_b} j^2 + \hbar^2 \left(\frac{1}{2I_a} - \frac{1}{2I_b} \right) j_a^2 \quad (3)$$

where j^2 is the square of the angular momentum that satisfies the relation $j^2 = j_a^2 + j_b^2 + j_c^2$ and I_a and I_b are the principal moments of inertia. The wave functions $|jkm\rangle$ of a symmetric top molecule are defined by three quantum numbers, where k denotes the projection of j along the C_{3v} -axis of the body-fixed reference and m is its projection on the z -axis of the space-fixed frame of reference. The energies of the rotational levels are given by :

$$E_{j,k} = B j(j+1) + (A - B) k^2 \quad (4)$$

where B and A are the rotational constants which are equal to 0.2850 cm⁻¹ and 5.3083 cm⁻¹ (El Idrissi et al. 2001) respectively. Due to the identical nuclear spin of hydrogen atoms, we distinguish two independent forms of propyne: *ortho*-CH₃CCH (or, $A-$) and *para*-CH₃CCH (or, $E-$). The rotational levels associated to the propyne molecule are characterized by $k = 3n \pm 1$ for *para*-CH₃CCH and $k = 3n$ for *ortho*-CH₃CCH (n being integer).

It is important to note that the *ortho* to *para* transitions are strictly forbidden in such non-reactive collisions. Therefore, the scattering computations can be carried out separately for each nuclear spin species. The small values of the rotational constants

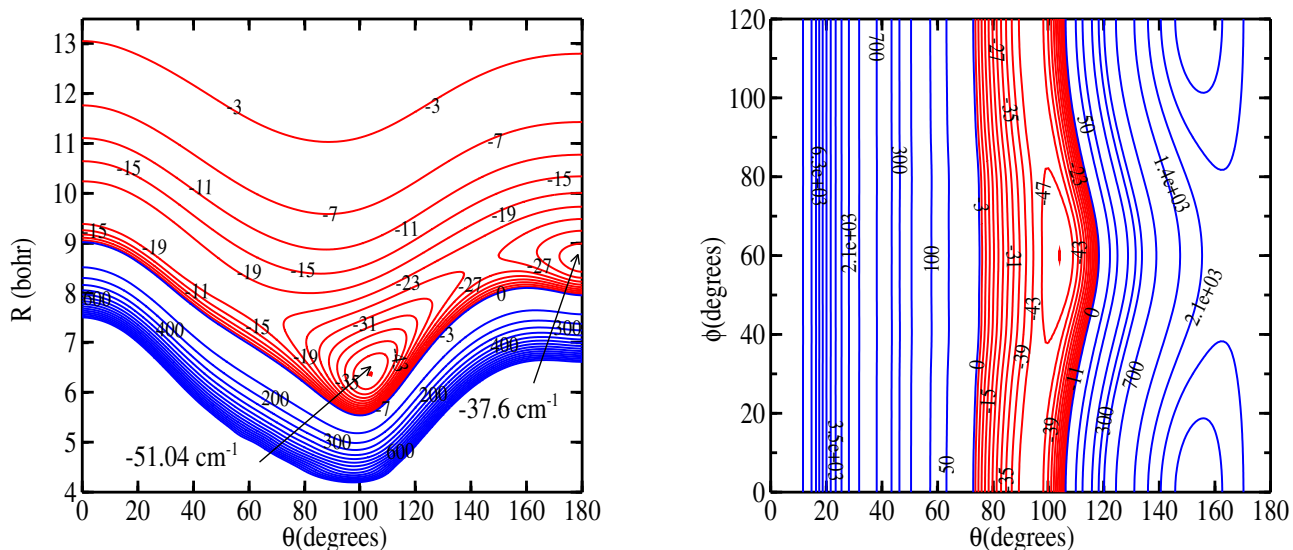


Fig. 3: Two-dimensional contour plots of the interaction potential of the $\text{CH}_3\text{CCH-He}$ van der Waals complex. The left panel depicts the 3D-PES as a function of θ and R at $\phi=60^\circ$, while the right panel shows the PES as a function of ϕ and θ at $R=6.6a_0$. For each panel, the blue (red) contours represent the positive (negative) parts of the potential (in unit of cm^{-1}).

A and B lead to a complex rotational structure with a high density of rotational levels. In the ISM, CH_3CCH is usually detected via transitions between highly excited states, e.g. 21_k to 20_k , $k=0, \dots, 7$ (Calcutt et al. 2019). This implies that cross sections of $\text{CH}_3\text{CCH-He}$ need to be carried out using a large rotational basis set, which limit the possibility of employing a full quantum-mechanical dynamics methods for scattering calculations.

3.1. Cross sections

The main focus of this paper is the study of the collisional (de-)excitation of CH_3CCH by He atoms. Cross sections for rotationally inelastic transitions of *para* and *ortho*- $\text{CH}_3\text{CCH-He}$ were carried out using the time-independent close-coupling (CC) method up to $E_{\text{tot}} \leq 100 \text{ cm}^{-1}$ and the coupled state (CS) approximation for total energies ranging from $100 \leq E_{\text{tot}} \leq 600 \text{ cm}^{-1}$. The scattering calculations were carried out using the Manolopoulos (1986) propagator to solve the coupled differential equations implemented in the MOLSCAT computer code. To keep computational time under control, we start by testing the integrator parameters, *STEPS* and the size of the rotational basis set N_{lev} , which were adjusted to ensure convergence of the rotational cross-sections over the entire energy range. Hence, the integration limits of the scattering computations were fixed at $R_{\text{min}}=3.5a_0$ and $R_{\text{max}}=50a_0$. The *STEPS*-parameter is set to 100 for $E_{\text{tot}} \leq 50 \text{ cm}^{-1}$, 70 for $E_{\text{tot}} \in [50, 100] \text{ cm}^{-1}$, 50 for $100 \leq E_{\text{tot}} \leq 200 \text{ cm}^{-1}$ and 30 for $E_{\text{tot}} \in [200, 600] \text{ cm}^{-1}$. All these propagator parameters were fixed by carrying out convergence tests. Furthermore, the size of the rotational basis set was optimized in order to include in the scattering computations all open channels along with a few closed channels.

For *ortho*- CH_3CCH , the number of rotational levels N_{lev} considered for our calculations was taken as: $N_{\text{lev}}=55$ (up to $j_k=24_3$ with an energy of 216.24 cm^{-1}) for total energies $E_{\text{tot}} \leq 50 \text{ cm}^{-1}$, $N_{\text{lev}}=80$ (up to $j_k=31_3$ with an energy of 327.98 cm^{-1}) for total energies $50 \text{ cm}^{-1} \leq E_{\text{tot}} \leq 100 \text{ cm}^{-1}$, and $N_{\text{lev}}=155$ (up

to $j_k=49_0$ with an energy of 698.39 cm^{-1}) for $102 \text{ cm}^{-1} \leq E_{\text{tot}} \leq 600 \text{ cm}^{-1}$. For *para*- CH_3CCH , we take $N_{\text{lev}}=105$ (up to $j_k=11_7$ with an energy of 283.79 cm^{-1}) for total energies $E_{\text{tot}} \leq 100 \text{ cm}^{-1}$, $N_{\text{lev}}=160$ (up to $j_k=37_2$ with an energy of 420.88 cm^{-1}) for total energies $100 \leq E_{\text{tot}} \leq 200 \text{ cm}^{-1}$, $N_{\text{lev}}=185$ (up to $j_k=38_4$ with an energy of 502.83 cm^{-1}) for total energies $202 \leq E_{\text{tot}} \leq 300 \text{ cm}^{-1}$ and $N_{\text{lev}}=215$ (up to $j_k=19_{10}$ with an energy of 610.65 cm^{-1}) for total energies $305 \leq E_{\text{tot}} \leq 600 \text{ cm}^{-1}$.

We attribute a value of 0.05 \AA^2 to the off-diagonal tolerance which determines the maximum value of the total angular momentum (J) that needs to be taken into account. Finally, given that the total angular momentum J is a quantity preserved, the integral cross section was obtained by summing partial wave contributions.

We calculated rotational cross sections for total energy ranging from 0.1 to 600 cm^{-1} . To do so, the energy grid was tuned to describe all the resonances in the cross sections and to cover the entire energy range required to compute collisional rates accurately up to 100 K . We used an energy step dE of 0.2 cm^{-1} for energies below 50 cm^{-1} , 0.5 cm^{-1} for energies between 50 cm^{-1} and 100 cm^{-1} , 2 cm^{-1} for energies between 100 cm^{-1} and 200 cm^{-1} , 5 cm^{-1} for energies between 200 cm^{-1} and 400 cm^{-1} , and 10 cm^{-1} for energies between 400 cm^{-1} and 600 cm^{-1} .

For kinetic energies where resonances become negligible ($E_c \geq 100 \text{ cm}^{-1}$), the calculations using CC method, in the fully converged limit, turned out to be impractical and would require an inordinate amount of computing time, thus we explored using the CS approximation to save time calculation. The CS approximation is indeed expected to be reliable at high kinetic energies (Phillips et al. 1996). We examined the accuracy of CS computations by direct comparison to CC ones as presented in Table 1 at a total energy of 100 cm^{-1} . As can be seen in Table 1, the relative error between CC and CS cross sections for selected transitions does not exceed 10% for $E_{\text{tot}}=100 \text{ cm}^{-1}$ with a disk occupancy and CPU time for the CC calculations that are several times larger than CS ones. We conclude that for $\text{CH}_3\text{CCH-He}$

Table 1: Comparison between CC and CS cross sections (in Å²) for the excitation of *para* CH₃CCH by He for total energies $E_{\text{tot}} = 100 \text{ cm}^{-1}$ with $N_{\text{lev}} = 80$.

Energy	$j_k \rightarrow j'_k$	CC	CS	Error
$E = 100 \text{ cm}^{-1}$	$1_1 \rightarrow 2_1$	4.0361	3.9202	2.8%
	$3_1 \rightarrow 4_1$	3.0956	3.1104	0.4%
	$5_1 \rightarrow 6_1$	2.9126	3.0719	0.6%
	$7_1 \rightarrow 9_1$	11.9612	11.8952	0.5%
	$3_2 \rightarrow 5_2$	14.4978	15.1471	4.4%
	$4_1 \rightarrow 5_2$	3.6750	3.7966	3.3%
	$9_1 \rightarrow 10_1$	2.7101	2.8221	7.8%
	$6_2 \rightarrow 9_2$	1.6051	1.7571	9.4%

collisions, the CS method can be used for total energies larger than 100 cm^{-1} .

Figure 4 shows examples of the kinetic energy dependence of collisional cross sections for the rotational excitation of *para*-CH₃CCH-He (right panel) and *ortho*-CH₃CCH-He (left panel) for some dipolar ($\Delta j = 1$) and quadrupolar ($\Delta j = 2$) transitions with $\Delta k = 0$. These figures underline the importance of using a sufficiently fine energy grid to correctly describe the resonances, especially for $E_c \leq 50 \text{ cm}^{-1}$. The cross sections for these transitions increase above the threshold at which these transitions open until achieving a maximum and then decrease as the collision energies increase. The cross-sections exhibit many Feshbach and shape resonances at kinetic energies below 50 cm^{-1} . This is due to the formation of quasi-bound states into the potential well depth before dissociation of the collisional complex.

Figure 4 reveals the existence of a strong even Δj propensity rule at almost all collision energies for CH₃CCH-He. The largest cross sections (in magnitude) are found for transitions with $\Delta j = 2$ that is, 1_0-3_0 , 2_0-4_0 and 3_0-5_0 for *ortho*-CH₃CCH-He and for the transitions 1_1-3_1 , 2_1-4_1 , and 3_1-5_1 for *para*-CH₃CCH-He. These propensity rules can be explained by exploring the shape of the PES, as the symmetry of the interaction potential will promote transitions with even $|\Delta j|$. Furthermore, this propensity rule can be understood by examining the radial terms $V_{lm}(R)$ described in Fig. 2. Cross sections with $|\Delta j| = 2$ are mainly caused by the V_{20} term, which is the dominant anisotropic term for CH₃CCH-He, hence, the magnitude of cross section corresponding to transitions with $|\Delta j| = 2$ are larger than for other transitions.

Propensity rules that favor even values of $|\Delta j|$ were already observed for the excitation of other symmetric top molecules with C_{3v} symmetry by He atoms, such as CH₃CN (Ben Khalifa et al. 2022) and SiH₃CN (Naouai et al. 2021). Figure 4 only illustrates cross sections for *para* and *ortho*-CH₃CCH-He and for transitions with $\Delta j = 0$, the same behavior is also observed for other values of Δk .

4. Rate coefficients

Calculated state-to-state rotational cross sections were used to compute the corresponding rate coefficients for the collisions of *ortho*- and *para*- type levels of methyl acetylene with He atoms by averaging over the collision energy (E_c).

$$k_{i \rightarrow f}(T) = \left(\frac{8}{\pi \mu \beta} \right)^{\frac{1}{2}} \beta^2 \int_0^{\infty} E_c \sigma_{i \rightarrow f}(E_c) e^{-\beta E_c} dE_c \quad (5)$$

where $\beta = 1/k_B T$ and k_B , T and $\mu = 3.638773549 \text{ au}$ are the Boltzmann constant, the kinetic temperature and the collision reduced mass, respectively.

In this work, the state-to-state cross sections calculated for total energy up to 600 cm^{-1} can be used to compute rate coefficients for transitions among the first 60 *ortho* levels (up to $j_k = 13_6$, $E_{\text{rot}} = 232.554 \text{ cm}^{-1}$) and 60 *para* levels (up to $j_k = 10_5$, $E_{\text{rot}} = 156.862 \text{ cm}^{-1}$) for kinetic temperature between 5 and 100 K. This complete set of (de-)excitation rate coefficients will be made available online on the EMAA (<https://emaa.osug.fr> and <https://dx.doi.org/10.17178/EMAA>) and BASECOL (Dubernet et al. 2023) databases for line radiative transfer studies.

Figure 5 displays plots of the quenching rate coefficients of CH₃CCH-He as a function of kinetic temperature for selected $\Delta j = 2$ transitions accompanied by $\Delta k = 0, 1$ and 3. These plots show that the order of magnitude of rate coefficients associated to transitions with $\Delta k = 0$, is larger than those with $\Delta k > 0$. The largest rate coefficients are found for the transitions: 5_3-3_3 , 6_3-4_3 and 7_3-5_3 for *ortho*-CH₃CCH-He and 4_2-2_2 , 5_2-3_2 and 6_2-4_2 for *para*-CH₃CCH-He. The rate coefficients for $\Delta j = 2$ transitions are seen to vary only weakly with temperature in the range investigated here. However, for $\Delta j = 1$ transitions (not shown), a stronger variation is observed with a decrease of the rate coefficients from 5 K to about 30 K, and a slow increase at higher temperature. To conclude, transitions with even $|\Delta j|$ and $|\Delta k| = 0$ are more favorable compared to those with $|\Delta j|$ and $|\Delta k| \neq 0$. These results correspond to those already observed at the level of the cross sections (see Fig. 4).

To the best of our knowledge, no collisional rates for the excitation of CH₃CCH were available in literature and the rate coefficients for CH₃CN were sometimes used in radiative transfer models to approximate the excitation of propyne in astrophysical media (Mauersberger et al. 1991). To assess the validity of such an approach in the collisional studies, we performed a comparison of CH₃CCH-He and CH₃CN-He collisional rate coefficients, computed recently by Ben Khalifa et al. (2023) with the same level of theory for both the construction of the PES as well as for the scattering dynamics. We present this comparison in Fig. 6 for transitions between the first 50 *ortho* levels and 50 *para* levels of CH₃CCH and CH₃CN at temperature $T = 100 \text{ K}$. One can see that collisional rate coefficients for the dominant transitions ($k > 10^{-11} \text{ cm}^3 \text{ s}^{-1}$, corresponding to $|\Delta k| = 0$ transitions) of both species agree within a factor of 2, however, we observe important differences for the smaller collisional rates with relative differences that reach a factor of 5. These differences show that independent calculations have to be performed for each molecule as the rate coefficients cannot be assumed to be equal.

The collisional rate coefficients obtained for the CH₃CCH-He and CH₃CN-He species allow us to predict that their excitation in the astrophysical environments is different. Therefore, a radiative transfer study must be carried out for CH₃CCH using its respective set of collisional rate coefficients to obtain an accurate abundance of propyne.

It is important to emphasize that this comparison is only for collisional excitation by He atoms, while the dominant collider in the ISM is H₂ molecule. At present, no collisional data is available for either CH₃CCH-H₂ or CH₃CN-H₂. In this case, one usually scales all rate coefficients for excitation by He atoms by a single factor to account for the mass difference between He and H₂, but the accuracy of such an approach is known to be limited.

5. Application

In the interstellar medium, the intensities of the emission lines are proportional to the population of the energy levels of the molecule. The evolution of these populations is based on colli-

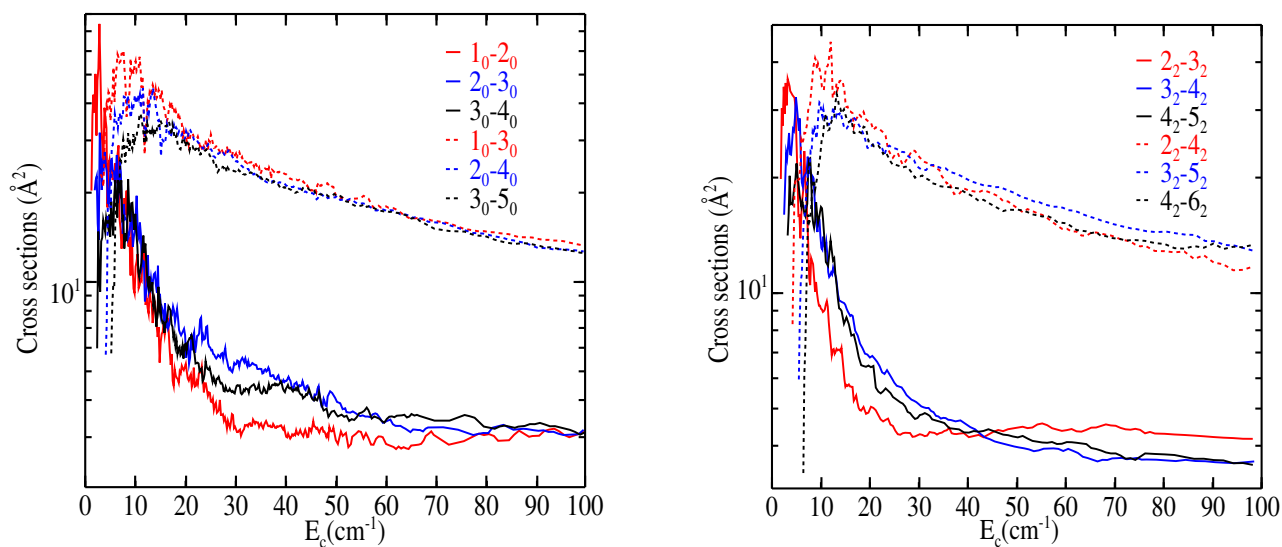


Fig. 4: Kinetic energy dependence of the rotational excitation cross sections $j_k \rightarrow j'_k$ of *ortho*-CH₃CCH-He (left panel) and *para*-CH₃CCH-He (right panel) in collision with He for $\Delta j = 1$ and $\Delta j = 2$ transitions while $\Delta k = 0$.

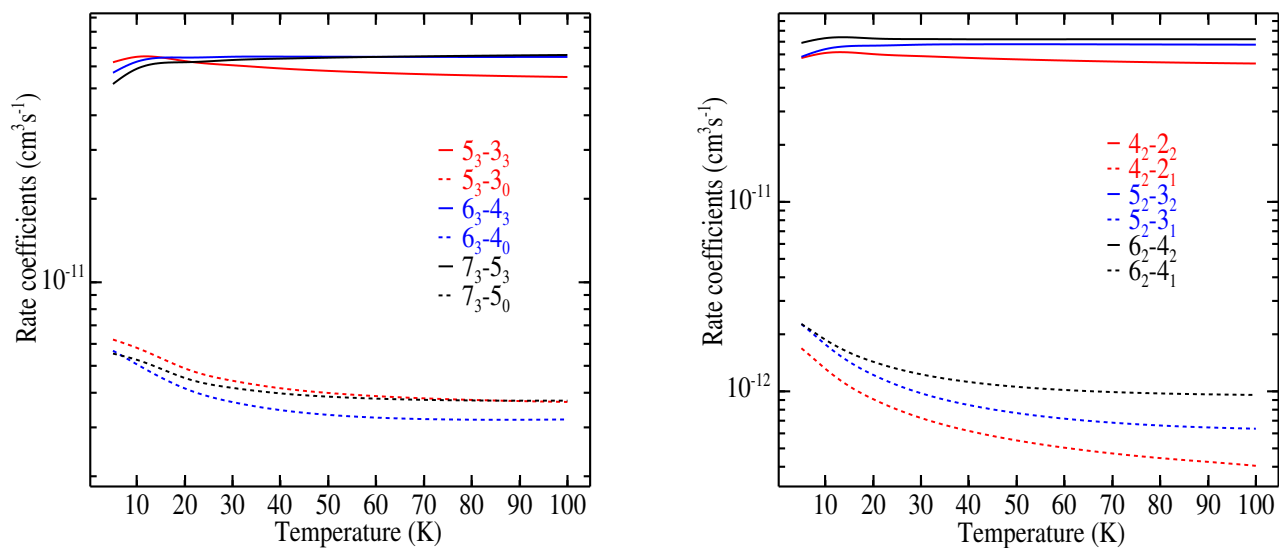


Fig. 5: Temperature dependence of the rotational excitation rate coefficients $j_k \rightarrow j'_k$ of *ortho*-CH₃CCH-He (left panel) and *para*-CH₃CCH-He (right panel) in collision with He atom for $\Delta j = 2$ and $\Delta k = 0, 1$ and 3 .

sional and radiative processes that are governed by collisional rate coefficients and radiative Einstein coefficients, respectively. The knowledge of these two sets of data allows one to perform a radiative transfer computation for the propyne molecule using the Radex (Van der Tak et al. 2007) computer code.

Non-LTE radiative transfer computations were performed using the escape probability approximation. Our collisional rate coefficients (from 5 to 100 K) were combined with spectroscopic data from the Cologne Data base for Molecular Spectroscopy portal (Müller et al. 2005). In practice, we have computed the excitation (T_{ex}) and brightness (T_{B}) temperatures for the

transitions $j_k=6 \rightarrow 4$ with $k=0,1,2$ and 3 at 102.5 GHz which are usually detected in astrophysical clouds (Andron et al. 2018). To do so, we scaled the CH₃CCH-He rates by a factor of 1.39 to approximate the rate coefficients that *para*-H₂($j=0$) would induce and we fixed the cosmic microwave background, the line width and the column density of propyne at 2.73 K, 2.1 km.s⁻¹ (Andron et al. 2018) and 10⁻¹⁴ cm⁻², respectively. Finally, we vary the volume density of the molecular hydrogen from 10² cm⁻³ to 10⁸ cm⁻³ to examine the behaviour of the excitation of CH₃CCH under and out of LTE conditions.

We display in Fig. 7, the variation of the excitation temperature

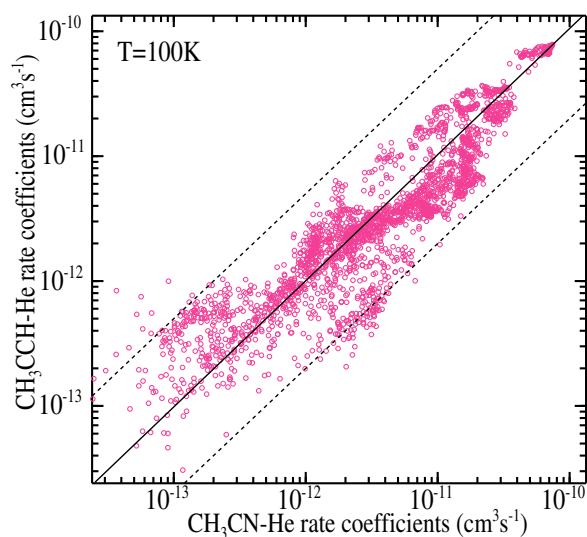


Fig. 6: Comparison between *ortho* and *para* CH₃CCH-He and CH₃CN-He rate coefficients at $T = 100$ K. The diagonal line corresponds to equal rate coefficients and the dashed line to the difference of a factor of 5.

of CH₃CCH for selected kinetic temperatures of 20, 50 and 100 K. We observe a supra-thermal effect at $T = 50$ and 100 K for H₂ densities between 10^4 and 10^6 cm⁻³, where the excitation temperature is larger than the kinetic temperature. At low H₂ density ($n_{H_2} < 10^4$ cm⁻³), the medium is dilute and the excitation temperature is given by the cosmic background temperature ($T_{ex} = T_{CMB} = 2.73$ K), while at high density ($n_{H_2} > 10^6$ cm⁻³), when the collisional excitation processes becomes more important, the T_{ex} tends asymptotically to the kinetic temperature where LTE conditions are reached. From these plots, we observe that the LTE is reached for volume densities above 10^6 cm⁻³.

6. Conclusion

In this paper, the first 3D-PES for the interaction between CH₃CCH and He atoms was computed using the explicitly correlated coupled cluster theory [CCSD(T)-F12a] and the aug-cc-pVTZ basis set. The global minimum was found to correspond to a potential well depth of 51.04 cm⁻¹ and an equilibrium intermolecular separation of 6.3 bohr. This interaction potential was used to compute rotationally-inelastic cross sections for transitions between the first 60-*ortho* and 60-*para* levels of CH₃CCH in collision with He atoms in time-independent close-coupled and coupled states quantum scattering computations. Rotational cross sections were calculated as a function of the total energy up to 600 cm⁻¹.

By thermally averaging the cross sections over the collision energy, collisional rates were computed for temperatures relevant to interstellar conditions, from 5 K to 100 K.

We have compared the new set of collisional rates of CH₃CCH-He with those for CH₃CN-He. This comparison shows that collisional rate coefficients are different by up to a factor of 5. Consequently, we must use the appropriate collisional rates of CH₃CCH to study the excitation of propyne in the interstellar

medium. We therefore recommend the use of these set of collisional rates in non-LTE models of CH₃CCH excitation.

We have also used the new set of rate coefficients in a simple radiative transfer model to assess their impact on four observed transitions. This study shows that the propyne lines are not thermalized and non-LTE models should be employed to analyse its emission spectra.

Acknowledgements. MBK thanks H. da Silva, Jr for help with HPC computing. JL acknowledges support from KU Leuven through grant no. C14/22/082. The scattering calculations presented in this work were performed on the VSC clusters (Flemish Supercomputer Center), funded by the Research Foundation-Flanders (FWO) and the Flemish Government.

References

- Agúndez, M., Fonfría, J. P., Cernicharo, J., Pardo, J. R., & Guélin, M. 2008, *Astronomy & Astrophysics*, 479, 493
- Andron, I., Gratier, P., Majumdar, L., et al. 2018, *Monthly Notices of the Royal Astronomical Society*, 481, 5651
- Ben Khalifa, M., Dagdigian, P., & Loreau, J. 2023, *Monthly Notices of the Royal Astronomical Society*, 523, 2577
- Ben Khalifa, M., Dagdigian, P. J., & Loreau, J. 2022, *J Phys Chem A*, 126
- Boys, S. F. & Bernardi, F. 1970, *Molecular Physics*, 19, 553
- Buhl, D. & Snyder, L. E. 1973, in *Molecules in the galactic environment*
- Burgdorf, M., Orton, G., van Cleve, J., Meadows, V., & Houck, J. 2006, *Icarus*, 184, 634
- Calcutt, H., Willis, E., Jørgensen, J., et al. 2019, *Astronomy & Astrophysics*, 631, A137
- De Graauw, T., Feuchtgruber, H., Bezaud, B., et al. 1997, *Astronomy and Astrophysics*, v. 321, p. L13-L16, 321, L13
- Dubernet, M.-L. et al. 2023, *Astronomy & Astrophysics*, doi:10.1051/0004-6361/202348233
- Dunning Jr, T. H. 1989, *The Journal of chemical physics*, 90, 1007
- El Idrissi, M., Liévin, J., Herman, M., Campargue, A., & Graner, G. 2001, *Chemical physics*, 265, 273
- Fayolle, E. C., Öberg, K. I., Garrod, R. T., van Dishoeck, E. F., & Bisschop, S. E. 2015, *Astronomy & Astrophysics*, 576, A45
- Fouchet, T., Lellouch, E., Bézard, B., et al. 2000, arXiv preprint astro-ph/0002273
- Gratier, P., Majumdar, L., Ohishi, M., et al. 2016, *The Astrophysical Journal Supplement Series*, 225, 25
- Gratier, P., Pety, J., Guzmán, V., et al. 2013, *Astronomy & Astrophysics*, 557, A101
- Gubbels, K. B., van de Meerakker, S. Y. T., Groenenboom, G. C., Meijer, G., & van der Avoird, A. 2012, *J. Chem. Phys.*, 136, 074301
- Guzmán, A. E., Guzmán, V. V., Garay, G., Bronfman, L., & Hechenleitner, F. 2018, *The Astrophysical Journal Supplement Series*, 236, 45
- Guzmán, V. V., Pety, J., Gratier, P., et al. 2014, *Faraday Discussions*, 168, 103
- Herbst, E. 2017, *International Reviews in Physical Chemistry*, 36, 287
- Hickson, K. M., Wakelam, V., & Loison, J.-C. 2016, *Molecular Astrophysics*, 3, 1
- Hutson, J. M. & Green, S. 1995, MOLSCAT computer code, version 14, Distributed by Collaborative Computational Project 6, Warrington, UK: Daresbury Laboratory
- Knizia, G., Adler, T. B., & Werner, H.-J. 2009, *The Journal of chemical physics*, 130, 054104
- Loreau, J., Liévin, J., Scribano, Y., & van der Avoird, A. 2014, *J. Chem. Phys.*, 141, 224303
- Loreau, J. & Van der Avoird, A. 2015, *The Journal of Chemical Physics*, 143, 184303
- Lovas, F. J., Johnson, D. R., Buhl, D., & Snyder, L. E. 1976, *The Astrophysical Journal*, 209, 770
- Manolopoulos, D. 1986, *The Journal of chemical physics*, 85, 6425
- Mauersberger, R., Henkel, C., Walmsley, C., Sage, L., & Wiklind, T. 1991, *Astronomy and Astrophysics (ISSN 0004-6361)*, vol. 247, no. 2, July 1991, p. 307-314., 247, 307
- Mebel, A. M., Landera, A., & Kaiser, R. I. 2017, *The Journal of Physical Chemistry A*, 121, 901
- Müller, H. S., Schlöder, F., Stutzki, J., & Winnewisser, G. 2005, *Journal of Molecular Structure*, 742, 215
- Naouai, M., Jrad, A., Badri, A., & Najar, F. 2021, *Monthly Notices of the Royal Astronomical Society*, 507, 5264
- Öberg, K. I., Boamah, M. D., Fayolle, E. C., et al. 2013, *The Astrophysical Journal*, 771, 95
- Parker, D. S. & Kaiser, R. I. 2017, *Chemical Society Reviews*, 46, 452

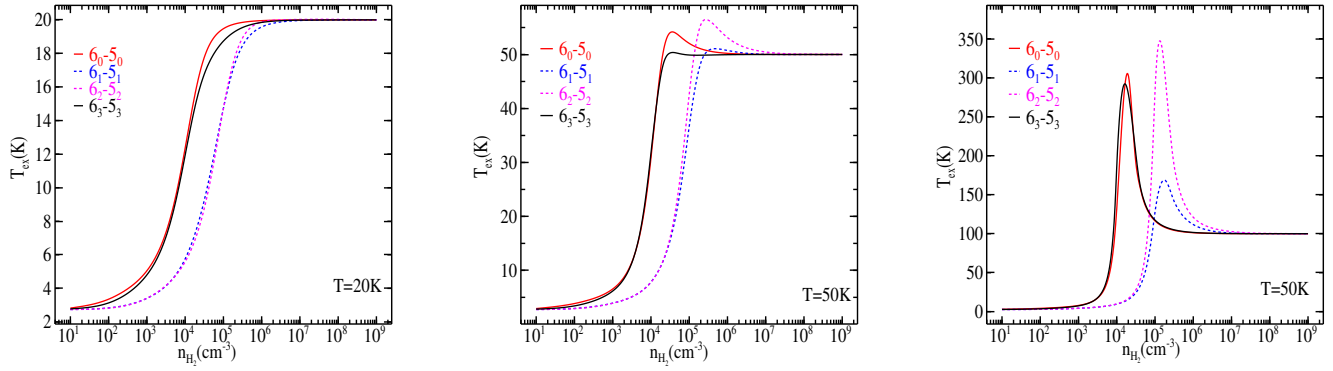


Fig. 7: Excitation temperature of CH_3CCH for the transitions $j_k \rightarrow j'_k$, with $j = 6$, $j' = 5$ and $k = k' = 0$ or 2 (*para*- CH_3CCH) and $k = k' = 0$ or 3 (*ortho*- CH_3CCH) as a function of the H_2 density for three kinetic temperature (20 K, 50 K and 100 K) and a column density of 10^{14} cm^{-2} .

- Phillips, T. R., Maluendes, S., & Green, S. 1996, *Astrophysical Journal Supplement* v. 107, p. 467, 107, 467
- Qiu, J., Zhang, J., Zhang, Y., Jia, L., & Tang, X. 2020, *Astronomy & Astrophysics*, 634, A125
- Schiff, H. & Bohme, D. K. 1979, *The Astrophysical Journal*, 232, 740
- Schmidt, D. & Ziurys, L. 2019, *The Astrophysical Journal Letters*, 881, L38
- Teanby, N., Irwin, P., de Kok, R., et al. 2009, *Icarus*, 202, 620
- Turner, B., Terzieva, R., & Herbst, E. 1999, *The Astrophysical Journal*, 518, 699
- Van der Tak, F., Black, J. H., Schöier, F., Jansen, D., & van Dishoeck, E. F. 2007, *Astronomy & Astrophysics*, 468, 627
- van Dishoeck, E. F., Blake, G. A., Jansen, D. J., & Groesbeck, T. 1995, *Astronomical Journal*, 447, 760
- Vastel, C., Ceccarelli, C., Lefloch, B., & Bachiller, R. 2014, *The Astrophysical Journal Letters*, 795, L2
- Werner, H.-J., Knowles, P. J., Knizia, G., et al. 2015, MOLPRO, version 2015.1, a package of ab initio programs, <http://www.molpro.net>
- Wlodarczak, G., Bocquet, R., Bauer, A., & Demaison, J. 1988, *Journal of Molecular Spectroscopy*, 129, 371